

Supplementary Information for “Raman spectroscopy as a versatile tool for studying the properties of graphene”

Andrea C. Ferrari¹, Denis M. Basko²¹Cambridge Graphene Centre, Cambridge University,
9 JJ Thomson Avenue, Cambridge, CB3 0FA, UK²Université Grenoble 1/CNRS, LPMMC UMR 5493, 25 rue des Martyrs, 38042 Grenoble, France

S1. RAMAN SCATTERING

Raman scattering¹ is the inelastic scattering of photons by phonons, Fig. S1. A photon impinging on a sample creates a time-dependent perturbation of the Hamiltonian. Due to the photon fast changing electric field, only electrons respond to the perturbation. The electronic wave-functions of the perturbed system can be written as a linear combination, with time-dependent coefficients, of all the wave-functions of the unperturbed system. The perturbation introduced by a photon of energy $\hbar\omega_L$ increases the total energy to $E_{GS} + \hbar\omega_L$, where E_{GS} is the ground state energy. In general, $E_{GS} + \hbar\omega_L$ does not correspond to a stationary state, therefore the system is said to be in a virtual level. In classical language, a virtual level corresponds to a forced oscillation of the electrons with a frequency ω_L . Once the photon realizes that the system has no stationary state of energy $E_{GS} + \hbar\omega_L$, it leaves this unstable situation. We can formally consider the photon as being emitted by the perturbed system, which jumps back to one of its stationary states.

Rayleigh scattering takes place when the system returns to its initial state, and the frequency of the emitted photon remains the same as the incident one. This is also called *elastic scattering*, and all that can happen to the photon is a change in its propagation direction. Still, Rayleigh or elastic scattering can give useful information^{2,3}. Graphene is indeed one of the most successful examples³, since elastic scattering is now commonly used to image the flakes and derive the number of layers^{3,4}. The presence of an appropriate spacer, such as the typical 300nm SiO₂ over Si⁵, can enhance significantly the incident field amplitude within graphene, thus its visibility^{3,4}. Had not been for this effect, that enabled to see even a single layer graphene (SLG) simply using an optical microscope⁵, the whole graphene research field may never have started.

Raman scattering happens when, with a much lower probability than Rayleigh scattering, the photon can lose part of its energy in the interaction process, thus exiting the sample with a lower energy $\hbar\omega_{Sc}$. This corresponds to the Stokes (S) process. Since the sample has to return to a stationary state, the energy loss must correspond to a phonon energy, $\hbar\omega_L - \hbar\omega_{Sc} = \hbar\Omega$. If the incoming photon finds the sample in an excited vibrational state, and after the interaction the system returns to its ground level, the photon can leave the crystal with an increased energy $\hbar\omega_{Sc} = \hbar\omega_L + \hbar\Omega$. This corresponds to the Anti-Stokes

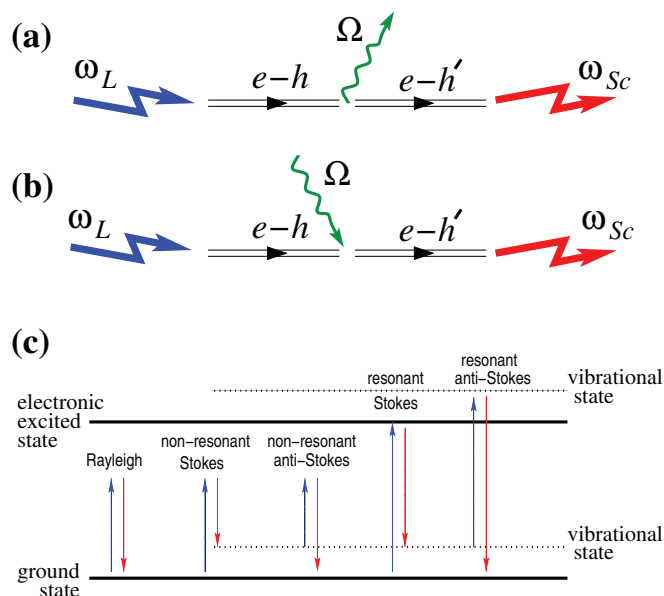


Figure S1. **Raman Scattering.** (a) Stokes. An incoming photon ω_L excites an electron-hole pair $e-h$. The pair decays into a phonon Ω and another electron-hole pair $e-h'$. The latter recombines, emitting a photon ω_{Sc} . (b) Anti-Stokes. The phonon is absorbed by the $e-h$ pair. (c) Rayleigh and Raman scattering in resonant and non resonant conditions.

(AS) process. Given that S is the most probable⁶, the vast majority of Raman spectra in literature are S measurements plotting the intensity of the scattered light as a function of the difference between incident and scattered photon energy, the so called "Raman shift". Even though the Raman shift units should be those of energy, it is historically plotted in cm^{-1} . These can be converted in meV using the relation $1 \text{ meV} = 8.0655447 \text{ cm}^{-1}$. The S/AS ratio depends on the sample temperature⁶, and is a very popular method to monitor it. However, in graphene and nanotubes, the nature of the resonant process has to be carefully considered when comparing S/AS intensities, since the resonance windows for incident and scattered photons are different^{7,8}. Not doing so gives wrong temperature estimations.

Non-resonant Raman scattering is when $E_{GS} + \hbar\omega_L$ does not correspond to a stationary state, as is indeed the case for most materials. If the excitation is selected to match a specific energy level⁶, then the process is *resonant*, and the intensities are strongly enhanced, as a

result of the greater perturbation efficiency. In a quantum mechanical description, this corresponds to a vanishing denominator in the perturbation theory expression for the transition amplitude. Resonant Raman scattering has been intensely studied since the 1960-1970s for semiconductors (see Ref. 9 for a review).

For light in the infrared (IR) to ultraviolet (UV) spectral range, the main scattering mechanism involves electronic excitations as intermediate states, rather than direct photon-phonon coupling, because the laser energy is large compared to the phonon energy¹⁰. This is even more so for carbon allotropes, since they are non-polar. Thus, the study of the Raman spectra can shed light on the behavior of electrons^{11,94}, and complement transport measurements. The Raman intensities calculations in solids date back to the 1960s, with free electron-hole (e - h) pairs¹² and excitons¹³ as intermediate states. Graphene differs from usual semiconductors in several aspects, with important consequences. First, the linear gapless electronic dispersion implies resonances for any ω_L . Second (related to the first), there are no excitons (i.e. real bound states of an electron and a hole). Third, in the IR-visible range, the electronic spectrum has approximately symmetric conduction and valence bands, while for semiconductors the difference between e and h effective masses m_e, m_h is usually of the order of m_e, m_h themselves, and often $m_h \gg m_e$ ⁶. Still, Raman scattering for semiconductors with equal masses was previously studied, both theoretically and experimentally. In indium halides (such as InBr, InI) $m_e = m_h$ and their Raman spectra were found to exhibit peaks up to the 20th order; even-order peaks being more intense than odd-order ones¹⁴. This was assigned to full resonance¹⁵, which is of direct relevance for even-order peaks in graphene.

If \mathbf{k}_L and $\omega_L = ck_L$ are the wave vector and frequency of the incoming photon, \mathbf{k}_{Sc} and $\omega_{Sc} = ck_{Sc}$ those of the scattered photon (c being the speed of light), and \mathbf{q} and $\Omega_{\mathbf{q}}^{\nu}$ those of a phonon belonging to a branch ν , then energy and momentum conservation give:

$$\omega_L = \omega_{Sc} \pm \Omega_{\mathbf{q}}^{\nu}, \quad (\text{S1})$$

$$\mathbf{k}_L = \mathbf{k}_{Sc} \pm \mathbf{q}. \quad (\text{S2})$$

In the S process a phonon is created (“+”), in AS one is annihilated (“−”). Typical Raman experiments are conducted in the 1064 – 229 nm range, corresponding to 1.2 – 5.4 eV^{16–18}. Since the lattice parameter, a , is of the order of a few Å (~ 1.42 Å in graphene¹⁹), $k_L, k_{Sc} \ll \pi/a$, the magnitude of a zone boundary wavevector. Then, from Eqs. (S1,S2), $q \ll \pi/a$, i.e. in first-order scattering only phonons near Γ ($\mathbf{q} \approx \mathbf{0}$) are measured. This is referred to as the *fundamental Raman selection rule*.

The emission of two phonons with opposite wavevectors can *always* satisfy the fundamental selection rule: $\mathbf{q} + (-\mathbf{q}) = \mathbf{0}$. Since each individual \mathbf{q} *a priori* can be arbitrary, all phonons may contribute to a multi-phonon process. Thus, in principle, the multiphonon Raman spectrum will reproduce the main features of the phonon density of states (PDOS), and can be used to derive important information on the phonon branches, as done, e.g., in hexagonal boron nitride, h-BN²⁰. Graphene is yet again special: only very few intense features are seen, not corresponding to the PDOS maxima^{21,22}, due to the peculiar nature of the resonant process and the electron-phonon and electron-electron interactions^{11,21,22}. h-BN, albeit with an hexagonal lattice as graphene, is a wide gap semiconductor and, unless Raman spectroscopy is performed in the deep UV^{20,23}, is not resonant.

In general, Raman scattering can be described by perturbation theory⁶. For an n -phonon process we have an $(n + 2)$ order matrix element:

$$\mathcal{M} = \sum_{s_0, \dots, s_n} \frac{\langle f | \hat{H}^{\text{em}} | s_n \rangle \langle s_n | \hat{H}^{\text{ph}} | s_{n-1} \rangle \dots \langle s_1 | \hat{H}^{\text{ph}} | s_0 \rangle \langle s_0 | \hat{H}^{\text{em}} | i \rangle}{(\hbar\omega_L - E_n + i\Gamma_n/2) \dots (\hbar\omega_L - E_1 + i\Gamma_1/2)(\hbar\omega_L - E_0 + i\Gamma_0/2)} \quad (\text{S3})$$

with $|i\rangle$ the initial state (incident photon with frequency ω_L , polarized along a unit vector \mathbf{e}_{in}), $|f\rangle$ the final state (scattered photon with frequency ω_{Sc} and polarization \mathbf{e}_{out} , and n phonons left in the crystal), while s_k , $k = 0, \dots, n$, label the intermediate states where no photons are present, but an $e - h$ pair is created and k phonons emitted. E_k and Γ_k/\hbar are the energies and decay rates of these intermediate states. \hat{H}^{em} and \hat{H}^{ph} are the Hamiltonians describing the interaction of electrons with the electromagnetic field and with phonons. In practice, for $n > 1$, the enumeration of all possible intermediate states is cumbersome, so that a diagrammatic

scattering formalism is useful for a systematic analysis of all relevant terms. According to the number of vanishing denominators in Eq. (S3), the process can be classified as doubly-resonant (DR) or triply-resonant (TR). Higher orders are also possible in multiphonon processes.

Each term in the sum of Eq. (S3) can be viewed as the complex amplitude of the corresponding elementary process with given intermediate states. These amplitudes may add up in phase or out of phase, which would correspond to constructive or destructive quantum interference. For non-interacting electrons in a defect-free crystal, the summation over the intermediate states in Eq. (S3) is reduced to an integration over the electronic

momentum. In the presence of defects, the momentum is not a good quantum number for electronic wave functions. Still, if the density of defects is not very high, their effect on the wave functions can be treated perturbatively. This corresponds to introducing more intermediate states, as well as matrix elements of electron-defect scattering, $\langle s_{i+1} | \hat{H}_{def} | s_i \rangle$, in Eq. (S3), and again integrating over the electronic momentum. This procedure treats electron scattering on defects analogously to scattering on phonons, so that a defect can be viewed as a phonon with zero frequency.

Given \mathcal{M} , one should sum its square over the phonon wavevectors, either with fixed total energy, to obtain the frequency-resolved intensity $I(\omega)$, or over all energies, to get the frequency-integrated peak intensity A :

$$I(\omega_{Sc}) \propto \int |\mathcal{M}|^2 \delta(\Omega_{\mathbf{q}_1}^{\nu_1} + \dots + \Omega_{\mathbf{q}_n}^{\nu_n} - \omega_{Sc}) d^2 \mathbf{q}_1 \dots d^2 \mathbf{q}_n, \quad (\text{S4})$$

$$A = \int_{\omega_{Sc} \in \text{peak}} I(\omega_{Sc}) d\omega_{Sc} \propto \int |\mathcal{M}|^2 d^2 \mathbf{q}_1 \dots d^2 \mathbf{q}_n, \quad (\text{S5})$$

where $\mathbf{q}_1, \dots, \mathbf{q}_n$ are the wave vectors of the emitted phonons, ν_1, \dots, ν_n their branch labels, and $\Omega_{\mathbf{q}_1}^{\nu_1}, \dots, \Omega_{\mathbf{q}_n}^{\nu_n}$ are their frequencies. The frequency-integrated intensity is more robust with respect to various perturbations of the phonon states. Indeed, for dispersionless undamped phonons, Ω^ν , the shape of the n -phonon peak is $\propto \delta(\omega_{Sc} - n\Omega^\nu)$ with zero width, infinite height, but well-defined area. If the phonons are allowed to decay (e.g, into other phonons due to anharmonicity²⁴ or into e - h pairs due to electron-phonon coupling, EPC²⁵), the δ -peak is broadened into a Lorentzian, but the area is preserved, as the total number of phonon states cannot be changed by such perturbations. If phonons have a weak dispersion, then states with different momenta contribute at slightly different frequencies. This may result in an overall shift and a non-trivial peak shape, but frequency integration across the peak means counting all phonon states, as in the dispersionless case. Thus, the frequency-integrated intensity is preserved as long as \mathcal{M} is not changed significantly by the perturbation. The latter holds when the perturbation is smaller than the energy scale determining \mathcal{M} . This is usually dominated by electronic broadening, and often larger. Converting energy into time by the uncertainty principle, if the process is faster than phonon decay, the total number of photons emitted within the given peak (i. e., integrated over frequency across the peak), is not affected by phonon decay, although their spectral distribution can be.

Raman spectroscopy can also probe scattering of photons by electronic excitations. In pristine graphene electronic excitations have a continuous structureless spectrum²⁶, which does not lead to any sharp features. However, in a strong magnetic field, B , when the electronic spectrum consists of discrete Landau levels, the electronic inter-Landau-level excitations give rise to sharp B -dependent peaks in the Raman spectrum^{27–30}.

S2. INTERFERENCE-ENHANCED RAMAN SCATTERING

In general, the Raman intensity depends on the square of the incident field amplitude⁶. Thus it can also be enhanced by a proper choice of substrate and spacer, resulting in the so-called Interference Enhanced Raman Scattering (IERS). This is a common occurrence in graphene^{31,32}, and the reasons are analogous to those enabling its visibility on a substrate^{31,32}. Due to interference, the enhancement varies as a function of both excitation and emission wavelengths, being in principle different for different Raman peaks. The transfer matrix method can be used to evaluate the effect of substrate interference and sample absorption³³. First, the incident amplitude $E(x)$ in the sample is evaluated, as a function of sample thickness x . The Raman absorption at depth x is proportional to $|E(x)|^2$. Next, the emissivity $E_R(x)$ from depth x at the corresponding Stokes-shifted frequency is calculated³³. The Raman intensity is then proportional to $\int_{x=0}^d |E(x)|^2 |E_R(x)|^2 dx$. This shows that changes with respect to an “intrinsic” $I(2D)/I(G)$ are small for a SLG on 300 nm SiO₂ measured at 514 nm. Thus, it is safe to compare this ratio amongst different samples and assign its variation to doping or other external perturbations. However, different substrates or wavelengths, may result in IERS changes of $I(2D)/I(G)$ even for the same sample. On the other hand, an optimal interference-enhancing substrate could be designed, with uniform enhancement across different Raman bands (so that their ratios do not change), at the same time ensuring high optical visibility.

S3. SURFACE-ENHANCED RAMAN SCATTERING

Surface Enhanced Raman Scattering (SERS) exploits surface plasmons, induced by the incident field in metallic nanostructures, to increase the intensity³⁴. In principle, even a single metallic nanostructure, e.g., a nanotip, can induce SERS, giving rise to the so-called tip-enhanced Raman scattering (TERS)³⁵. The key feature of TERS is its capability of optical sensing with high spatial resolution beyond the light diffraction limits³⁵.

Graphene is an ideal model system to study SERS. Ref.33 did SERS by depositing patterned particles of different sizes and spacings on SLG. Taking into account the surface plasmon resonance near-fields, the Raman enhancement scales with particle cross section, fourth power of Mie enhancement, and inversely with the tenth power of the separation between particle centre and graphene³³, pointing to thin nanodisks to achieve the highest SERS for two dimensional (2d) materials³³.

S4. RAMAN SCATTERING IN GRAPHITE AND GRAPHENE: HISTORY AND NOMENCLATURE

Figure 1(e) in the main text shows the Raman spectrum of pristine and defected graphene, while Figure 4(f) in the main text compares the Raman spectra of graphite, nanotubes and amorphous carbons.

It is very instructive to summarize the main steps in the historical development of the understanding of the graphite Raman spectrum. This was first reported in 1970 in the seminal work of Tuinstra and Koenig (TK)³⁶. They assigned the mode at $\sim 1580\text{cm}^{-1}$ to the high frequency E_{2g} Raman allowed optical phonon. They also measured in defected and nanocrystalline graphite a second peak at $\sim 1350\text{cm}^{-1}$. They assigned it to an A_{1g} breathing mode at \mathbf{K} , activated by the relaxation of the Raman fundamental selection rule³⁶. This was done following both the “molecular” and “solid state” routes.

The assignment is straightforward considering carbons as big molecules³⁷. Similar bands are seen in all polyaromatic hydrocarbons³⁸. The higher frequency band is due to bond stretching of sp^2 pairs in both rings and chains, while the lower frequency one is due breathing modes of sp^2 atoms in rings^{17,36,38}, see Fig. 1(c) of the main text. Thus, in absence of rings, the latter would be absent, while the former is present in any carbon materials, ranging from carbon chains, to hard amorphous carbons¹⁸, Fig. 4(f) of the main text. Except for UV excitation, the Raman spectra of carbons are dominated by the sp^2 sites, because visible light resonates with the π states, the cross section for graphite and graphene at 514nm being ~ 55 times higher than diamond³⁹. Only for diamond, or samples with a significant fraction of diamond phase, the diamond sp^3 peak at 1332cm^{-1} is seen⁴⁰. In amorphous carbons, the C–C sp^3 vibrations can be seen for UV excitation at $\sim 1060\text{cm}^{-1}$ (usually called T peak, from Tetrahedral)¹⁷.

The “solid-state” interpretation has been debated for the past 40 years. TK tried to combine the “molecular” and “solid-state” approaches as follows. First they considered graphite nanocrystals as big aromatic molecules, and noted that the only new Raman active modes would have A_{1g} symmetry, Fig. 1(c) of the main text. Then they looked at the graphene lattice and noted that the only Brillouin Zone (BZ) points with high enough symmetry to give an A_{1g} mode were \mathbf{K} and \mathbf{K}' . They were left with a problem: the fundamental Raman selection rule forbids $\mathbf{q} \neq \mathbf{0}$ phonons. Since they observed the $\sim 1350\text{cm}^{-1}$ band to increase with decreasing crystal size, they assumed that phonon confinement in ever smaller nanocrystals would progressively lift the selection rule. From the uncertainty principle $\Delta q \Delta x \sim \hbar$, thus $\Delta q \propto 1/\Delta x$, and the smaller the crystal size Δx , the larger Δq . However, this picture had a flaw. To activate BZ boundary A_{1g} phonons requires $\Delta x \sim$ lattice spacing, in disagreement with the observation of the $\sim 1350\text{cm}^{-1}$ band in crystals as large as $\sim 100\text{nm}$ ³⁶. Also, confinement could not ex-

plain why the A_{1g} mode was more intense than others closer to Γ (all these modes could in principle be activated, as happens in other nanomaterials⁴¹).

TK did not give any names to these Raman peaks. The first nomenclature was proposed by Vidano and Fishbach in 1977⁴². Since they observed strong lines at ~ 1580 and $\sim 2700\text{cm}^{-1}$ in pristine graphite, while other bands at ~ 1350 and $\sim 1620\text{cm}^{-1}$ only appeared in defected graphite, they called the former G, G' (from Graphite) and the latter D, D' (from Disorder). Nemanich and Solin detected a sharp band at $\sim 3250\text{cm}^{-1}$ in pristine graphite⁴³, as well as a weaker one at $\sim 2450\text{cm}^{-1}$ ⁴⁴. They also noted a further peak at $\sim 2950\text{cm}^{-1}$ in defected samples⁴⁴, later named D'' by Vidano et al.⁴⁵. In 1979 Nemanich and Solin, by polarization dependent measurements, assigned all peaks between 2300 and 3250cm^{-1} in pristine graphite as overtones. In particular, they indicated that the $\sim 2450\text{cm}^{-1}$ peak was also an overtone. They also noted that, with defects, combinations of phonons with different wavevectors become allowed, since the requirement to have opposite wavevector was progressively lifted. They thus assigned the $\sim 2950\text{cm}^{-1}$ band as D + D', rather than D + G, due to the phonon density of states (PDOS) maximum at $\sim 1620\text{cm}^{-1}$ for the LO branch, see Fig. 1d of the main text. In 1981 Vidano *et al.* studied the excitation energy dependence, and confirmed G' to be the D overtone, and the $\sim 3250\text{cm}^{-1}$ peak the D' overtone, since these shifted at twice the rate of their fundamentals⁴⁵. They stressed those bands behaved differently from G, that did not move with excitation energy. They also noted the energy dependence of the $\sim 2950\text{cm}^{-1}$ peak was consistent with D+D' or D+G.

Thus, by 1981 it was clear that, while the Raman-allowed first-order G peak did not shift with excitation energy, the “defect-related” bands D, D', their overtones and combinations did. This ruled out their assignment to PDOS maxima, activated by confinement, since a PDOS maximum cannot change as a function of excitation energy, being an intrinsic material property. The symmetry and phonon branches that originated D and D' were also known. The next step would have been to figure out the reason for this shift.

However, subsequent works claimed D derived from a PDOS maximum around \mathbf{M} or \mathbf{K} ⁴⁶, even though phonons at \mathbf{M} do not have the required symmetry, PDOS maxima are inconsistent with the D and G' dispersion, and the dimension of the crystals in Ref. 36 was too big to activate zone boundary phonons by confinement only. These issues and discrepancies remained unresolved, and even ignored, for the following 16 years. A similar fate happened for other main peaks. E.g., although it was clear the $\sim 3250\text{cm}^{-1}$ band is not the G second order, a large number of papers (to date) still call it 2G.

In 1998 Pocsik et al.¹⁶ repeated the experiments of Vidano *et al.*⁴⁵ over a much larger excitation energy range, as shown in Fig. 1(g) of the main text, and, not surprisingly, found the same results. To try and explain the excitation energy dependence they proposed a “new” res-

onant process, whereby a strong enhancement of the Raman cross-section would happen for a phonon of wavevector \mathbf{q} , when this equals the wavevector \mathbf{k} of the electronic transition excited by the incident photon (the so-called $\mathbf{k}=\mathbf{q}$ “quasi-selection rule”¹⁷). However, the physical reason for this “quasi-selection rule” was unclear (it does not exist in Raman scattering) and did not yet explain why, amongst all phonons satisfying it, only those on one particular branch would be seen. Given the experimental $\text{Disp}(D) \sim 50\text{cm}^{-1}/\text{eV}$,¹⁶ only a phonon branch upshifting from \mathbf{K} would satisfy the “quasi-selection” rule, since the linear electron dispersions would select larger k with increasing excitation energy, thus larger q . However, the TO branch, corresponding to the A_{1g} phonon at \mathbf{K} , had the opposite behavior in the most popular calculations at the time⁴⁶. Pocsik et al. thus identified the LO branch, with E symmetry at \mathbf{K} , as responsible for the D peak, in contrast with TK. In 1999 Ref. 47 repeated the experiments of Ref. 16, and reached the same conclusions⁴⁷. Thus, 30 years after Ref. 36, we were back to square one. A selection rule had to be “invented” to explain the D peak, and it was assigned to a different branch and symmetry, in contrast with the “molecular” view³⁷. There was also no convincing explanation why a zone boundary phonon would be active.

In 2000, Thomsen and Reich suggested double resonance (DR) as the activation mechanism⁴⁸: i) the laser excites an $e-h$ pair with wavevector \mathbf{k} defined by resonance with the π, π^* bands; ii) this is followed by electron-phonon scattering with exchanged momentum \mathbf{q} near \mathbf{K} ; iii) defect back-scattering of the electron to the initial \mathbf{k} ; iv) $e-h$ recombination. This process allows for an exchange of a large phonon momentum, while satisfying energy conservation at any step, thus the fundamental Raman selection rule. A defect is also needed, consistent with the observations of TK. Notably DR was first proposed by Baranov *et al.* in 1987⁴⁹, who called it “double coupled resonance”, but somehow went unnoticed, until Ref. 48 was out. We discuss in the main text the important ramifications of this mechanism, and the current understanding of the processes responsible for the various Raman peaks, as well as the issues still open.

Besides the activation mechanism, the phonons around \mathbf{K} are crucial for the correct D assignment, since $\text{Disp}(D)$ depends on the precise shape of these branches. Graphene has three branches around \mathbf{K} which could in principle contribute, see Fig. 1(d) of the main text. Following the suggestion of Pocsik et al.¹⁶ most authors^{16,47,48,50,51} assigned D to the LO branch stemming from the doubly degenerate $\sim 1200\text{cm}^{-1}$ E mode at \mathbf{K} , until 2004, when Ref.22 finally demonstrated the D phonons belonged to the TO branch starting from the A_{1g} mode at \mathbf{K} . Indeed, this branch has the largest EPC amongst \mathbf{K} phonons^{22,25} and is linearly dispersive close to \mathbf{K} , see Fig. 1(d) of the main text. A Kohn anomaly at \mathbf{K} ²² is the physical origin of this dispersion, in quantitative agreement with the measured $\text{Disp}(D)$, as shown in Fig. 1(g) of the main text.

In general, atomic vibrations are partially screened by electronic states. In a metal this screening can change rapidly for vibrations associated to certain BZ points, entirely determined by the shape of the Fermi surface. The consequent anomalous behavior of the phonon dispersion is called Kohn anomaly (KA)⁵². KA may occur only for wavevectors \mathbf{q} such that there are two electronic states \mathbf{k}_1 and $\mathbf{k}_2 = \mathbf{k}_1 + \mathbf{q}$ both on the Fermi surface⁵². In graphene, the gap between occupied and empty states is zero at \mathbf{K}, \mathbf{K}' , see Fig. 1(a) of the main text. Since $\mathbf{K}' = 2\mathbf{K}$ (up to a reciprocal lattice vector), these are connected by the vector \mathbf{K} (see Fig. 1(a) of the main text). Thus, KA can occur for $\mathbf{q} = \mathbf{\Gamma}$ or $\mathbf{q} = \mathbf{K}$ ²². Ref. 22 demonstrated that graphene has two significant KA’s for the $\mathbf{\Gamma}-E_{2g}$ and $\mathbf{K}-A_{1g}$ modes, see Fig. 1(a,d) of the main text. It is thus impossible to derive the precise shape of the phonon branches at $\mathbf{\Gamma}$ and \mathbf{K} by approaches based on a finite number of force constants, as often done^{37,50,51,53-55}. These results have also implications for nanotubes. Due to their reduced dimensionality, metallic tubes display much stronger KA than graphene, and folded graphene does not reproduce their phonon dispersions^{25,56}. The presence of KA explains the difference in the Raman spectra of semiconducting and metallic tubes^{25,56}.

The EPCs and phonons calculations of Ref. 22 were confirmed close to $\mathbf{\Gamma}$ by inelastic X-ray scattering^{57,58}, and by the measurement of FWHM(G) in graphite, graphene and nanotubes^{21,25,56,59}, once an-harmonic effects are taken into account^{21,24,59}. A further EPC renormalization and phonon softening happens at \mathbf{K} due to electron correlations^{11,50,60}. Note that the A_{1g} mode exactly at \mathbf{K} has zero EPC for the Raman process, thus only TO phonons away from \mathbf{K} , even if close to it, contribute to the D peak^{22,61}. Note as well that h-BN, even if with the same hexagonal lattice as SLG, does not have KAs, being a wide band-gap semiconductor²⁰.

The band at $\sim 2450\text{cm}^{-1}$ in Fig. 1(e) of the main text was first reported by Ref.44 in graphite, and suggested to be an overtone⁴⁴. Ref.44 stated that, since the product of any representation with itself always contains the identity, overtones are expected to have a contribution with polarization characteristics stronger in configurations which measure the diagonal components of the Raman tensor. Ref.44 then measured the cross polarized spectrum of graphite and observed that all the high energy modes, i.e. those at $\sim 2450\text{cm}^{-1}$, the 2D and 2D’, behaved in the same way, being much stronger than the G peak compared to parallel polarization. Refs.62–64 showed that this peak red-shifts with excitation energy, unlike the 2D and 2D’ blue-shift^{16,45}. Many alternative assignments have been put forward for this band over the years. Ref.17 suggested a contribution from the LA branch around the BZ edge. Refs.62–65 interpreted it as a combination of D and a phonon belonging to the LA branch, seen at $\sim 1100\text{cm}^{-1}$ for visible excitation in defected samples, and called D’ peak. Ref.66 assigned it as the non-dispersive overtone of the LO branch ex-

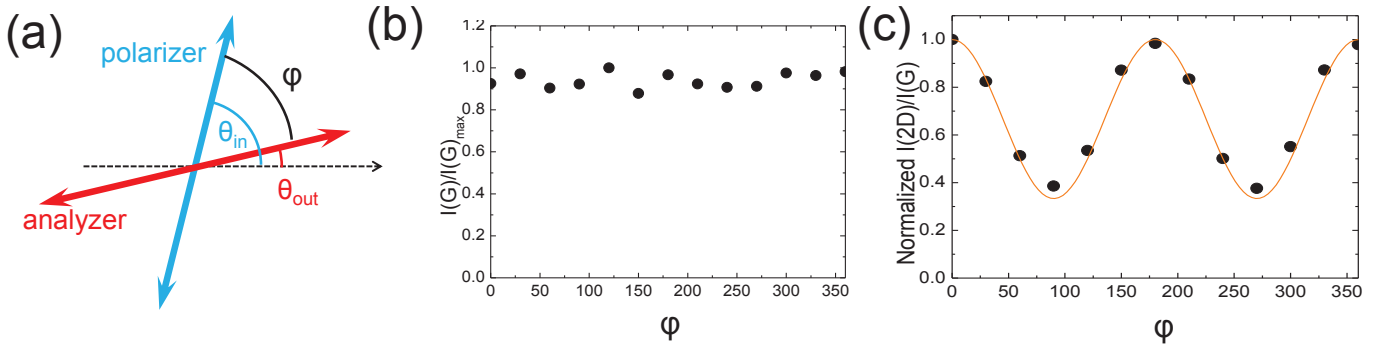


Figure S2. **Polarization.**(a) Geometry for polarized measurements. Normalized (b) $I(G)$ and (c) $I(2D)/I(G)$ as a function of angle between polarizer and analyzer.

actly at \mathbf{K} , and Ref.67 as a combination of LA and LO phonons. On one hand combinations of phonons with different energies do not correspond to a fully resonant process^{11,60}, and would be expected to be more dominant in the presence of defects, but this band, like 2D and 2D', is present in defect-free samples, see Fig. 1(e) of the main text, while overtones exactly at \mathbf{K} are non dispersive, in contrast with experiments⁶²⁻⁶⁴. On the other hand, as discussed in the main text, D and D'' have the same wave-vector, and their energy difference is of the order of the electron scattering rate. Thus, both 2D'' and D+D'' could contribute to this band, with D+D'' closer to the experiments⁶⁸⁻⁷⁰. We then assign it to D + D''.

To summarize, the current understanding is that the D peak is due to TO phonons around \mathbf{K} ^{17,36}, is active by DR^{48,49} and is strongly dispersive with excitation energy due to the KA at \mathbf{K} ²². Since the so-called G' band is in fact the D overtone, and has nothing to do with G, neither in terms of symmetry, nor in terms of phonon branch, nor in terms of Raman process, we²¹ renamed it 2D. Consequently the $\sim 3250\text{cm}^{-1}$ band is 2D', and the $\sim 2950\text{cm}^{-1}$ band is D + D'. Note that, due to resonance, in graphene (and nanotubes), it is easy to measure multiphonon peaks up to the 6th order^{62-64,71}. Our nomenclature allows one to simply assign all these bands: 4D, 6D, 4D', etc. With the previous names, the overtones and combinations would be confusing. It was also proposed to call D* the G' band, and G* the 2D', using "*" to indicate second order⁷². However, besides the problem of naming the multiphonon processes, G* is confusing since it would imply, for consistency, it being the G peak overtone, while it is in fact 2D'. G* is also often used to indicate the 2450cm^{-1} band⁶⁷, however, again, this has nothing to do with G, and this name conflicts with the use of G* for 2D'. Perhaps G' would be a more appropriate name for D', since this arises from a resonant process on the same branch giving rise to the G peak. However, it is also true that D' requires a defect and that its resonant Raman process has much in common with D, and nothing to do with G⁷³. The only drawback in calling 2D the $\sim 2700\text{cm}^{-1}$ band is that 2D is often used to mean "two-dimensional". We believe this issue to be minor,

since it is hard to confuse 2D, used for "two-dimensional", with the $\sim 2700\text{cm}^{-1}$ peak. For full clarity one can use 2d to indicate "two-dimensional". Furthermore, the nature of the 2D peak is so much related to the two dimensionality of graphene, to be not so unwarranted both share an acronym. Fig. 1(e) of the main text summarizes our nomenclature, for defect-free, or defected graphene.

S5. POLARIZATION DEPENDENCE

We now consider polarized excitation and detection, i.e. when the polarization vectors of incident and/or scattered light, \mathbf{e}^{in} , \mathbf{e}^{out} , are fixed, Fig. S2.

The $I(G)$ polarization dependence can be derived from symmetry^{74,75}. Its matrix element, described by the lattice displacement \mathbf{u} (see Fig.S3(d) for the geometry), is:

$$\mathcal{M}_G \propto (e_x^{\text{in}} e_y^{\text{out}} + e_y^{\text{in}} e_x^{\text{out}})u_x + (e_x^{\text{in}} e_x^{\text{out}} - e_y^{\text{in}} e_y^{\text{out}})u_y, \quad (\text{S6})$$

where the x direction is chosen to be perpendicular to the C-C bond. As long as the phonon frequency does not depend on the direction of \mathbf{u} (i.e., the two modes are degenerate), $I(G) \propto |\mathcal{M}_G|^2$, does not depend on the \mathbf{e}^{in} , \mathbf{e}^{out} directions, as shown experimentally in Fig.S2(b).

The $I(2D)$ and $I(2D')$ polarization dependence^{69,74,76,77} can be derived from the real-space Raman picture. The interband electron-photon matrix element for photon absorption/emission is $\propto [\mathbf{e}^{\text{in/out}} \times \mathbf{k}]$, where \mathbf{k} is the electron momentum counted from the Dirac point. Since both e and h momenta are parallel to the phonon momentum \mathbf{q} (counted from \mathbf{K} or $\mathbf{\Gamma}$ for 2D, or 2D'), the matrix element for the Raman process with emission of two phonons with momenta \mathbf{q} and $-\mathbf{q}$ is $\mathcal{M}_{\mathbf{q}} \propto [\mathbf{E}^{\text{in}} \times \mathbf{q}]$. The intensity is given by the integration of $|\mathcal{M}_{\mathbf{q}}|^2$ over the \mathbf{q} directions:

$$I(2D, 2D') \propto |\mathbf{e}^{\text{in}}|^2 |\mathbf{e}^{\text{out}}|^2 + 2(\mathbf{e}^{\text{in}} \cdot \mathbf{e}^{\text{out}})^2 \quad (\text{S7})$$

Thus, the intensity would depend on the relative orientation of \mathbf{E}^{in} and \mathbf{E}^{out} , being largest when parallel and smallest (by a factor ≈ 3) when perpendicular, and not on their orientation with respect to the crystal.

Fig.S2c plots the polarization dependence of $I(2D)/I(G)$ for SLG, in agreement with Eq.(S7). Note that Eq.(S7) is not sensitive to the weights with which different \mathbf{q} directions contribute. Since for each direction there are other two, oriented at $\pm 2\pi/3$, contributing in the same way, as required by symmetry, this is already sufficient to give Eq.(S7). The objective numerical aperture should also be taken into account when comparing with experiments.

For the D, D', the real-space picture is analogous to 2D, 2D'. Thus, one can expect the same 1/3 depolarization ratio. However, this should be taken with caution, as different types of defects can scatter electrons differently, which can significantly modify the picture. E.g., edges are defects, but give a different behavior, as discussed in the main text. For D + D' the backscattering condition is absent, so polarization memory should be weaker.

Thus far we considered both polarizer and analyzer present. The signal for unpolarized excitation is the sum of two signals for two orthogonal polarizations. The same for detection. Thus, when only one is present, there will be no dependence on polarizer/analyzer orientation.

S6. ELECTRIC FIELD AND DOPING

An important consequence of TR is the sensitivity of $A(2D)$ to the electronic inelastic scattering rate $2\gamma/\hbar$: $A(2D) \propto 1/\gamma^2$, according to Ref. 74 (see also Ref.69). γ has contributions from electron-phonon and electron-electron scattering, the latter increasing with carrier concentration (or Fermi energy, E_F): $\gamma = \gamma_{e-ph} + \gamma_{e-e}$. For weak doping, $|E_F| \ll \hbar\omega_L/2$, $\gamma_{e-e} = f|E_F|$, with the coefficient $f \sim 0.5 - 1$ determined by the dielectric environment^{11,78}. Thus, $A(2D)$ decreases as E_F moves away from the Dirac point^{79,80}. From the measured dependence, the two contributions to γ could be separated, giving an estimate for $\gamma_{e-ph} \sim 20 - 30$ meV at energies ~ 1 eV¹¹. Here it is important that the 2D peak is mostly contributed by electronic states near the $\mathbf{K} - \mathbf{M}$ direction, as discussed in the main text. Along this direction, the interband contribution to γ_{e-e} is suppressed by trigonal warping^{81,82}.

Several effects originate from the fact that phonon frequencies and decay rates have a contribution due to interaction with π electrons. Indeed, this determines the phonon slopes near $\mathbf{\Gamma}$ and \mathbf{K} , via KAs²². This also gives a dependence of phonon frequencies and decay rates on doping^{59,83,84} and on applied magnetic field^{85,86}. Doping results in E_F -dependent blue shift and narrowing of the G peak^{59,79,80,87} according to^{59,83,84}:

$$\hbar\Delta\text{Pos}(G)_{E_F} = \frac{\lambda_\Gamma}{2\pi} \left[|E_F| + \frac{\hbar\text{Pos}(G)_0}{4} \ln \left| \frac{2E_F - \hbar\text{Pos}(G)_0}{2E_F + \hbar\text{Pos}(G)_0} \right| \right], \quad (\text{S8})$$

$$\text{FWHM}(G)_{E_F} = \text{FWHM}(G)_0 \{ f_F[-\hbar\text{Pos}(G)_0/2 - E_F] - f_F[\hbar\text{Pos}(G)_0/2 - E_F] \} \quad (\text{S9})$$

where $f_F(E)$ is the Fermi-Dirac distribution at energy E , $\text{Pos}(G)_0$ and $\text{FWHM}(G)_0 = \lambda_\Gamma \text{Pos}(G)_0/4$ are the G peak position and width for zero doping, λ_Γ is the dimensionless EPC for the LO phonons at $\mathbf{\Gamma}$. The logarithmic singularity in SLG can be washed out by disorder. Nevertheless it was observed in both SLG⁵⁹ and, more clearly, in BLG^{80,88}. Note that $\text{FWHM}(G)_0$ and $\text{Pos}(G)_0$ can give an accurate measure of $\lambda_\Gamma \sim 0.03$ ^{11,22}. Measurement of $\text{Pos}(G)$ combined with $\text{FWHM}(G)$ can then be used to estimate doping of an arbitrary sample, e.g. due to charged impurities⁸⁹.

The above results apply to relatively weak doping, $|E_F|$ small compared to $\hbar\omega_L/2$. In the past few years, much higher doping levels have been achieved⁹⁰⁻⁹². One of the effects of high doping is on the G peak intensity, as can be understood from Fig. 2(a) of the main text. Doping changes occupations of electronic state and, since transitions from an empty state or to a filled state are impossible, it can effectively exclude some regions of \mathbf{k} from contribution to the Raman matrix element. Due to suppres-

sion of destructive interference, this leads to an enhancement of the G peak when $|E_F|$ matches $\hbar\omega_L/2$, as predicted theoretically⁷³ and observed experimentally^{90,91}.

The most dramatic effect of high doping is on the 2D peak, which is suppressed when the conduction band becomes filled at the energy probed by the laser⁹⁰⁻⁹². Fig.S3(a) plots the Raman spectra measured at 488, 514, 561, 593 and 633nm for a highly doped graphene sample⁹². $A(2D)/A(G)$ and $I(2D)/I(G)$ are plotted as a function of excitation energy in Fig. S3(b). The trend of these intensity ratios can be understood from Fig. S3(c). The frequencies of the absorbed and emitted photons ω_L, ω_{Sc} differ by $\text{Pos}(2D)$: $\omega_{Sc} = \omega_L - \text{Pos}(2D)$. There are three cases: (i) when $\omega_L, \omega_{Sc} > 2|E_F|/\hbar$, all processes are allowed and the 2D band is observed, (ii) when $\omega_{Sc} < 2|E_F|/\hbar < \omega_L$, the photon absorption is allowed but the phonon emission is excluded by Pauli blocking; (iii) when $\omega_L, \omega_{Sc} < 2|E_F|/\hbar$, both photon absorption and phonon emission are blocked. Therefore, only when $2|E_F|/\hbar < \omega_L - \text{Pos}(2D)$, the 2D band is observable.

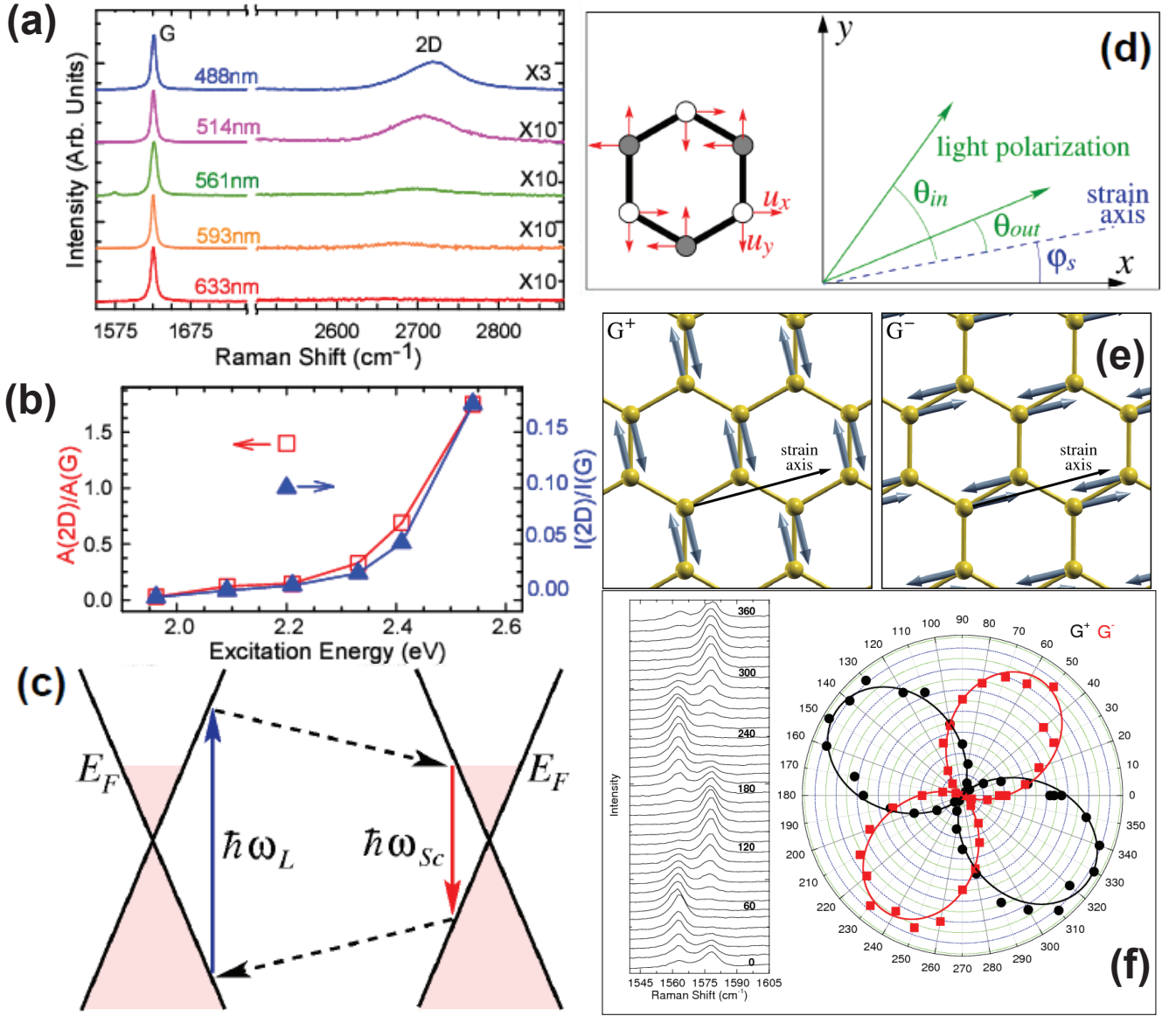


Figure S3. **Doping and strain**(a) Raman spectra of highly doped SLG measured at 488, 514 532, 561, 593 and 633nm, normalized to have the same $I(G)^{92}$. (b). $A(2D)/A(G)$ and $I(2D)/I(G)$ as a function of excitation energy⁹². (c) Schematic diagram of SLG band structure and 2D Raman processes in doped graphene. (d) Geometry for strain measurements. (e) G peak splitting by strain. (f) Sample orientation determined by polarized measurements under uniaxial strain.

Thus, the absence of the 2D band in the Raman spectra in Fig. S3(a) at 1.96eV (633nm) indicates that E_F should be larger than 0.81eV. From the sharp increase in $A(2D)/A(G)$ and $I(2D)/I(G)$ when $\hbar\omega_L$ increases from 2.21eV (561nm) to 2.09eV (593nm), one can deduce that $\hbar\omega_{Sc}$ corresponding to $\hbar\omega_L = 2.09$ eV is close to $2E_F$. A similar effect is expected on other DR and TR Raman peaks, such as D, D', 2D', D+D'', etc.

At sufficiently high doping, $E_F > E_L/2 - \hbar\Omega_q^{TO}$, an additional decay channel opens for the finite- q TO phonon: production of intraband electron-hole pairs⁹³, which results in an additional contribution to the width of the 2D

band, as observed in Ref.91.

S7. MAGNETIC FIELD

Several effects of the perpendicular magnetic field on Raman spectra of graphene have been observed in recent years. When a perpendicular magnetic field is applied, the electronic trajectories are no longer straight, but circular. This modifies the backscattering condition, so the emitted phonons have smaller momenta than those given by Eq.(2) of the main text. This results in a red shift

and additional 2D peak broadening⁹⁴.

The effect of coupling between π electrons and Γ phonons assumes a peculiar form when a sufficiently strong (10-30T) perpendicular magnetic field B is applied^{85,86}. The correction to the phonon frequency depends on the nature of the electronic states, and in a magnetic field the latter are quantized into discrete Landau levels with energies $E_n(B)$: $E_n(B) = (\text{sign } n)\sqrt{2|n|v_F^2 eB\hbar}$, $n = \dots, -1, 0, 1, 2, \dots$. The Γ phonons couple to electronic transitions $n \rightarrow n'$ between Landau levels n, n' , which satisfy the selection rule $|n| - |n'| = \pm 1$, thus having frequencies: $\hbar\Omega_m(B) = E_m(B) + E_{m+1}(B)$ for undoped graphene. At certain $B = B_m$ the resonance condition $\Omega_m(B) = \Omega_{\Gamma}$ is satisfied and, due to electron-phonon interaction, the phonon becomes strongly coupled to the electronic transition^{85,86}. This coupling manifests in a series of avoided crossings in $\text{Pos}(G)$ as a function of B near $B = B_m$ ^{29,30,95,96,99}, whose strength depends on the filling factor, as observed in Ref.99. Besides providing another EPC estimate, magneto-Raman can also probe the electronic Landau levels, from which v_F can be extracted. An analogous effect was predicted for BLG⁹⁷, and observed for four-layer graphene⁹⁸. Since the magneto-phonon resonance is strongly sensitive to the electronic band structure, its Raman spectrum is quite different for different number of layers, and thus can be used for its determination.

Raman spectroscopy can also probe scattering of photons by electronic excitations. In pristine graphene electronic excitations have a continuous structureless spectrum¹⁰⁰, which does not lead to any sharp features. However, in a strong magnetic field, when the electronic spectrum consists of discrete Landau levels, the electronic inter-Landau-level excitations give rise to sharp B -dependent peaks in the Raman spectrum (instead of a phonon, an e-h pair is emitted)^{27,28,101}. The selection rule for the Raman-active electronic transitions $n \rightarrow n'$ is $|n'| = |n|$ when excitation and detection have the same circular polarization, and $|n'| = |n| \pm 2$ for different ones. The Raman peaks are observed at frequencies $\hbar\Omega_m = 2E_m$ and $\hbar\Omega_m = E_m + E_{m+2}$, respectively^{29,30,102}

S8. UNIAXIAL AND BIAxIAL STRAIN

Strain arises when a crystal is compressed or stretched out of equilibrium. The stiffness tensor provides the constitutive relation between applied stress and strain. Tensile strain usually gives phonon softening, and the opposite for compressive strain. The rate of these changes is summarized in the Grüneisen parameters, which also determine the thermomechanical properties¹⁰³. Refs.104 and 105 subjected graphene to uniaxial strain. The doubly degenerate E_{2g} optical mode was shown to split in two components, one along the strain and the other perpendicular, Fig. S3(e). This leads to G peak splitting into two bands^{104,105}, named G^+ and G^- by analogy with the effect of curvature on the nanotube G peak⁵⁶. Both red-

shift with strain, and their splitting increases¹⁰⁴.

The Grüneisen parameter for the E_{2g} phonon, $\gamma_{E_{2g}}$, is defined as¹⁰³ $\gamma_{E_{2g}} = -(1/\Omega^{E_{2g}})(\partial\Delta\Omega_h^{E_{2g}}/\partial\varepsilon_h)$ where $\varepsilon_h = \varepsilon_{ll} + \varepsilon_{tt}$ is the hydrostatic component of the applied uniaxial strain, l is the longitudinal direction, parallel to the strain, and t is the direction transverse to it; $\Omega^{E_{2g}}$ is $\text{Pos}(G)$ at zero strain, and $\Delta\Omega_h^{E_{2g}}$ is the shift resulting from the hydrostatic component. The hydrostatic deformation preserves the symmetry of the crystal, so it does not lead to splitting. The shear deformation potential $\beta_{E_{2g}}$ is defined analogously^{104,106}: $\beta_{E_{2g}} = (1/\Omega^{E_{2g}})(\partial\Delta\Omega_s^{E_{2g}}/\partial\varepsilon_s)$, with $\varepsilon_s = \varepsilon_{ll} - \varepsilon_{tt}$ the strain shear component, and $\Delta\Omega_s^{E_{2g}}$ is the splitting due to shear. For uniaxial strain the G^\pm peaks shifts are^{104,106,107}:

$$\begin{aligned} \Delta\text{Pos}(G^\pm) &= \Delta\Omega_h^{E_{2g}} \pm \frac{\Delta\Omega_s^{E_{2g}}}{2} = \\ &= -\gamma_{E_{2g}}\Omega^{E_{2g}}(\varepsilon_{ll} + \varepsilon_{tt}) \pm \beta_{E_{2g}}\Omega^{E_{2g}}\frac{\varepsilon_{ll} - \varepsilon_{tt}}{2}. \end{aligned} \quad (\text{S10})$$

Ref.104 obtained $\partial\text{Pos}(G^+)/\partial\varepsilon \sim -10.8 \text{ cm}^{-1}/\%$, $\partial\text{Pos}(G^-)/\partial\varepsilon \sim -31.7 \text{ cm}^{-1}/\%$, $\partial\text{Pos}(2D)/\partial\varepsilon \sim -64 \text{ cm}^{-1}/\%$, $\partial\text{Pos}(2D')/\partial\varepsilon \sim -35 \text{ cm}^{-1}/\%$, $\gamma_{E_{2g}} \sim 1.99$, $\beta_{E_{2g}} \sim 0.99$.

The phonon displacements corresponding to the G^\pm peaks are orthogonal^{104,106,107}: E_{2g}^+ is perpendicular to the strain (thus experiencing smaller softening), and E_{2g}^- parallel, Fig. S3(e). With both polarizer and analyzer, the corresponding polarization vectors $\mathbf{e}_{in}, \mathbf{e}_{out}$ have definite orientations: $e_{in,out}^x = \cos(\theta_{in,out} + \varphi_s)$, $e_{in,out}^y = \sin(\theta_{in,out} + \varphi_s)$, where $\theta_{in,out}$ is the (known) angle between $\mathbf{e}_{in,out}$ and the strain axis, and φ_s is the (unknown) angle between the strain axis and the crystallographic axis. The matrix elements corresponding to emission of longitudinal and transverse phonons are proportional to $-\sin(\theta_{in} + \theta_{out} + 3\varphi_s)$ and $\cos(\theta_{in} + \theta_{out} + 3\varphi_s)$. The intensities are given by their squares:

$$\begin{aligned} I(G^-) &\propto \sin^2(\theta_{in} + \theta_{out} + 3\varphi_s), \\ I(G^+) &\propto \cos^2(\theta_{in} + \theta_{out} + 3\varphi_s). \end{aligned} \quad (\text{S11})$$

These allow to determine the sample orientation with respect to strain, Fig. S3(f).

It is important to consider that, while G probes the same centre-zone phonon under strain, this is not necessarily the case for 2D, 2D'¹⁰⁴. Any change in the band structure during strain will vary the actual phonons probed, as well as modifying the phonon frequencies. Thus, the relationship between phonon Grüneisen parameters and 2D, 2D' variation is in principle more complex than for G. Indeed, while biaxial strain does not move the relative positions of the Dirac cones, uniaxial strain changes them¹⁰⁸. This can have a significant influence in DR and TR processes. While 2D' is intravalley, 2D requires scattering from one cone to the other.

Thus, its wave vector is determined by the relative distance of the Dirac cones and by the laser energy. For a fixed excitation energy, one measures the combination of the 2D shift due to strain, and a possible additional shift due to the fact that the relative movement of the Dirac cones changes phonon wavevector. For an asymmetric movement this can lead to peak broadening¹⁰⁴, and splitting^{109,110}. The 2D broadening and splitting can give significant information on the nature of the TR process and the phonons involved, as well as on the band structure under strain, and the orientation of the strain axis with respect to the C–C bond^{104,105,109,110}. For 2D' the relative cone movement has no consequence. However, for 2D, 2D' other effects could be induced by Fermi and phonon group velocity renormalisation with strain.

Note that for biaxial strain at least the effects due to relative movement of Dirac cones are absent. Then, Raman experiments under biaxial strain are suited to measure the D Gruneisen parameter. Ref.111 performed these, and found no G or 2D peak splitting, as well as shifts and Gruneisen parameters in agreement with those deduced from the uniaxial measurements in Ref.104.

S9. TEMPERATURE

Due to anharmonic effects and phonon-phonon interactions, peak positions and FWHM depend on temperature T ¹¹². The investigation of the Raman peaks a function of T can provide valuable information on the anharmonic terms in potential energy and EPC^{24,59}. In graphene FWHM(G) depends on T in a peculiar way, slightly decreasing for low T , then increasing for $T > 700$ K. This can be written as^{24,59}: $\text{FWHM(G)}_T = \text{FWHM(G)}_T^{EPC} + \text{FWHM(G)}_T^{an}$ where FWHM(G)_T^{an} is the anharmonic contribution due to interaction with other phonons, and FWHM(G)_T^{EPC} the interaction with e - h pairs, given in Eq.(S9), while FWHM(G)_T^{an} was derived numerically²⁴. Eq.(S9) shows that the E_{2g} phonons damping due to decay in e - h pairs decreases with T due to partial Pauli blocking⁵⁹. Approximate expression for FWHM(G)_T^{an} can be derived assuming that phonons decay in 2 (3-phonon scattering) or 3 phonons (4-phonon scattering) with the same energy¹¹³. In this case $\text{FWHM(G)}_T^{an} = A \left[1 + \frac{2}{e^x - 1} \right] + B \left[1 + \frac{3}{e^y - 1} + \frac{3}{(e^y - 1)^2} \right]$ where $x = \hbar \text{Pos(G)}_0 / 2k_B T$ and $y = \hbar \text{Pos(G)}_0 / (3k_B T)$, and A, B are constants.

The temperature dependence of Pos(G) has a quasi-harmonic term, from thermal expansion, and an anharmonic one accounting for phonon-phonon scattering. Ref.113 proposed a simple model for the anharmonic phonon-phonon coupling including 3-phonon (3-ph) and 4-phonon (4-ph) processes. Then $\text{Pos(G)}_T = \text{Pos(G)}_0 +$

$\Delta \text{Pos(G)}_T$, where $\Delta \text{Pos(G)}_T = C \left[1 + \frac{2}{e^x - 1} \right] + D \left[1 + \frac{3}{e^y - 1} + \frac{3}{(e^y - 1)^2} \right]$, where C, D are constants, and x, y are the same as above.

S10. ISOTOPIC COMPOSITION

¹³C can be used to label graphene as well as nanotubes in order to measure fundamental properties or, e.g., to reveal growth processes¹¹⁴. The peak position of an isotope enriched sample is $\omega_{C_{13}} = \omega_{C_{12}} \cdot \sqrt{m_{12}/m_{13}}$ where $\omega_{C_{12}}$ and $\omega_{C_{13}}$ are the frequencies for full ¹²C and ¹³C samples, m_{12} and m_{13} the atomic masses of ¹²C and ¹³C. The isotopic shift is thus:

$$\frac{\partial \omega}{\partial C_{13}\%} = \frac{1}{100} \left(\omega_{C_{12}}^0 \cdot \sqrt{\frac{m_{12}}{m_{13}}} - \omega_{C_{12}}^0 \right) \approx -\frac{0.0392}{100} \omega_{C_{12}}^0 \quad (\text{S12})$$

Isotopic disorder also widens FWHM(G), with a maximum around 50% ¹³C.

S11. RAMAN AND GRAPHENE PROPERTIES

A. Raman and electrical transport

Raman spectroscopy is ideal to probe defects, electron-phonon and e-e interactions. Thus it can link sample quality to mobility^{115,116}, or EPC with current saturation^{8,117}.

B. Raman and heat transport

The Pos(G) temperature coefficient enabled the determination of thermal conductivity in single and multi-layer graphene^{118,119}.

C. Detection of heteroatoms

Functionalization and doping are an ever growing field. Any covalent bond gives a D peak. This is an *indirect* signature of C–H, C–O, C–F, C–N, C–Si, *etc.*, bonding^{17,120,121}, when visible Raman is performed, since the C–C sp^2 bonds always prevail¹⁷. UV Raman spectroscopy can directly probe the heteroatomic vibrations^{17,122}, and as such could be useful, especially for wide band gap compounds derived from graphene, and to probe SiC grown samples. Extreme care is needed with deep UV Raman since this can easily damage the sample and break the very bonds one wishes to study. UV Raman also allows to probe C–C sp^3 vibrations, otherwise overshadowed for visible excitation¹⁷.

¹ Landsberg, G. S. & Mandelshtam, L. I. Eine neue Erscheinung bei der Lichtzerstreuung in Krystallen. *Natur-*

wissenschaften **16**, 557 (1928); Raman, C. V. & Krish-

- nan, K. S. A New Type of Secondary Radiation. *Nature* **121**, 501 (1928).
- ² Sfeir, M. Y. *et al.* Optical Spectroscopy of Individual Single-Walled Carbon Nanotubes of Defined Chiral Structure. *Science* **312** 554 (2006).
 - ³ Casiraghi, C., *et al.* Rayleigh Imaging of Graphene and Graphene Layers. *Nano. Lett.* **7**, 2711–2717 (2007).
 - ⁴ Blake, P. *et al.* Making graphene visible. *Appl. Phys. Lett.* **91**, 063124 (2007).
 - ⁵ Novoselov, K. S. *et al.* Two-dimensional atomic crystals. *PNAS* **102**, 10451–10453 (2005).
 - ⁶ Yu, P. Y. & Cardona, M. *Fundamentals of Semiconductors* (Springer, Berlin, 2005).
 - ⁷ M. Oron-Carl & R. Krupke. Raman Spectroscopic Evidence for Hot-Phonon Generation in Electrically Biased Carbon Nanotubes. *Phys. Rev. Lett.* **100**, 127401 (2008).
 - ⁸ Berciaud, S. *et al.* Electron and Optical Phonon Temperatures in Electrically Biased Graphene. *Phys. Rev. Lett.* **104**, 227401 (2010)
 - ⁹ Martin, R. M. & Falicov, L. M. Resonance Raman scattering. In *Light Scattering in Solids I* (Ed. Cardona, M.) (Springer, Berlin, 1983).
 - ¹⁰ Born, M. & Huang, K. *Dynamical Theory of Crystal Lattices* (Oxford University Press, New York, 1954), p. 207.
 - ¹¹ Basko, D. M., Piscanec, S. & Ferrari, A. C. Electron-electron interactions and doping dependence of the two-phonon Raman intensity in graphene. *Phys. Rev. B* **80**, 165413 (2009).
 - ¹² Loudon, R. Theory of the first-order Raman effect in crystals. *Proc. Roy. Soc. (London) A* **275** (1963) 218–232. Loudon, R. Raman effect in crystals. *Adv. Phys.* **13**, 423–482 (1964).
 - ¹³ Birman, J. L. & Ganguly, A. K. Theory of Enhanced Raman Scattering and Virtual Quasiparticles in Crystals. *Phys. Rev. Lett.* **17** 647 (1966).
 - ¹⁴ Nakamura, K., Ohno, N., Yoshida, M. & Nakai, Y. Scattering spectra in orthorhombic indium bromide under resonant excitation. *Solid State Commun.* **36** 211–214 (1980).
 - ¹⁵ Lang, I. G. *et al.* Enhancement of multiphonon resonant Raman scattering of light in the case of equal effective masses of an electron and a hole. *Fiz. Tverd. Tela* **32** 3453 (1990).
 - ¹⁶ Pocsik, I., Hundhausen, M., Koos, M & Ley, L. Origin of the D peak in the Raman spectrum of microcrystalline graphite. *J. Non-Cryst. Solids* **227-230**, 1083–1086 (1998).
 - ¹⁷ Ferrari, A. C. & Robertson, J. Interpretation of Raman spectra of disordered and amorphous carbon. *Phys. Rev. B* **61**, 14095–14107 (2000); Resonant Raman spectroscopy of disordered, amorphous, and diamondlike carbon. *Phys. Rev. B* **64**, 075414 (2001).
 - ¹⁸ Ferrari, A. C. & Robertson, J. (eds), *Raman spectroscopy in carbons: from nanotubes to diamond*, Theme Issue, *Phil. Trans. Roy. Soc. A* **362**, 2267–2565 (2004).
 - ¹⁹ Charlier, J. C., Eklund, P. C., Zhu, J. & Ferrari, A. C. Electron and Phonon Properties of Graphene: Their Relationship with Carbon Nanotubes. *Topics Appl. Phys.* **111**, 673 (2008).
 - ²⁰ S. Reich *et al.* Resonant Raman scattering in cubic and hexagonal boron nitride. *Phys. Rev B* **71**, 205201 (2005).
 - ²¹ Ferrari, A. C., *et al.* Raman Spectrum of Graphene and Graphene Layers. *Phys. Rev. Lett.* **97**, 187401 (2006).
 - ²² Piscanec, S., Lazzeri, M., Mauri, F., Ferrari, A. C. & Robertson, J. Kohn Anomalies and Electron-Phonon Interactions in Graphite. *Phys. Rev. Lett.* **93**, 185503 (2004).
 - ²³ Arenal, R. *et al.* A Raman Spectroscopy of Single-Wall Boron Nitride Nanotubes. *Nano Lett.* **6**, 1812 (2006).
 - ²⁴ Bonini, N., Lazzeri, M., Marzari, N. & Mauri, F. Phonon Anharmonicities in Graphite and Graphene. *Phys. Rev. Lett.* **99**, 176802 (2007).
 - ²⁵ Lazzeri, M., Piscanec, S., Mauri, F., Ferrari, A. C. & Robertson, J. Phonon linewidths and electron-phonon coupling in graphite and nanotubes. *Phys. Rev. B* **73**, 155426 (2006).
 - ²⁶ Wallace, P. R. The Band Theory of Graphite. *Phys. Rev.* **71**, 622 (1948).
 - ²⁷ Kashuba, A., & Fal’ko, V. I. Signature of electronic excitations in the Raman spectrum of graphene. *Phys. Rev. B* **80**, 241404 (2009).
 - ²⁸ Kashuba, O. & Fal’ko, V. I., Role of electronic excitations in magneto-Raman spectra of graphene, *New. J. Phys.* **14** 105016 (2012).
 - ²⁹ Faugeras, C. *et al.* Magneto-Raman scattering of graphene on graphite: Electronic excitations and their coupling to optical phonons. *Phys. Rev. Lett.*, **107**, 036807, (2011)
 - ³⁰ Kim, Y. *et al.* Magnetophonon resonance in graphite: High-field Raman measurements and electron-phonon coupling contributions. *Phys. Rev. B*, **85**, 121403(R) (2012).
 - ³¹ Yoon, D, *et al.* Interference effect on Raman spectrum of graphene on SiO₂/Si. *Phys. Rev. B* **80**, 125422 (2009).
 - ³² Wang, Y. Y. *et al.* Interference enhancement of Raman signal of graphene. *Appl. Phys. Lett.* **92**, 043121 (2008).
 - ³³ Schedin, F. *et al.* Surface Enhanced Raman Spectroscopy of Graphene. *arXiv:1005.3268* (2010).
 - ³⁴ Kneipp, K., Moskovits, M. & Kneipp, K. (Eds.) *Surface-Enhanced Raman Scattering: Physics and Applications*, Springer-Verlag Berlin, (2006).
 - ³⁵ Hartschuh A. *et al.* High-Resolution Near-Field Raman Microscopy of Single-Walled Carbon Nanotubes *Phys. Rev. Lett.* **2003** 90, 095503.
 - ³⁶ Tuinstra, F. & Koenig, J. L. Raman Spectrum of Graphite. *J. Chem. Phys.* **53**, 1126–1130 (1970)
 - ³⁷ Mapelli, C. *et al.* Common force field for graphite and polycyclic aromatic hydrocarbons. *Phys. Rev. B* **60**, 12710–12725 (1999).
 - ³⁸ Castiglioni, C., Tommasini, M. & Zerbi, G. Raman spectroscopy of polyconjugated molecules and materials: confinement effect in one and two dimensions. *Phil. Trans. R. Soc. Lond. A* **362**, 2425–2459 (2004).
 - ³⁹ Wada, N. & Solin, S. A. Raman efficiency measurements of graphite. *Physica B*, **105** 353–356 (1981)
 - ⁴⁰ Ferrari, A. C. & Robertson, J. Origin of the 1150-cm⁻¹ Raman mode in nanocrystalline diamond. *Phys. Rev. B* **63**, 121405 (2001).
 - ⁴¹ Piscanec, S., *et al.* Raman spectroscopy of silicon nanowires. *Phys. Rev. B* **68**, 241312(R) (2003).
 - ⁴² Vidano, R. & Fischbach, D. B. New lines in the Raman spectra of carbons and graphite. *J. Am. Ceram. Soc.* **61**, 13–17 (1978).
 - ⁴³ Nemanich, R. J. & Solin, S. A. Observation of an anomalously sharp feature in the 2nd order Raman spectrum of graphite. *Solid State Comm.* **23**, 417–420 (1977).
 - ⁴⁴ Nemanich, R. J. & Solin, S. A. First- and second-order Raman scattering from finite-size crystals of graphite.

- Phys. Rev. B* **20**, 392 (1979)
- ⁴⁵ Vidano, R. P., Fishbach, D. B., Willis, L. J. & Loehr, T. M. *Solid State Comm.* **39**, 341–344 (1981).
- ⁴⁶ Al-Jishi, R. & Dresselhaus, G. Lattice-dynamical model for graphite. *Phys. Rev. B* **26**, 4514–4522 (1982).
- ⁴⁷ Matthews, M. J., Pimenta, M. A., Dresselhaus, G., Dresselhaus, M. S. & Endo, M. Origin of dispersive effects of the Raman D band in carbon materials. *Phys. Rev. B* **59**, R6585–R6588 (1999).
- ⁴⁸ Thomsen, C. & Reich, S. Double Resonant Raman Scattering in Graphite. *Phys. Rev. Lett.* **85**, 5214–5217 (2000).
- ⁴⁹ Baranov, A. V. *et al.* Interpretation of certain characteristics in Raman spectra of graphite and glassy carbon. *Opt. Spektrosk.* **62**, 1036 (1987).
- ⁵⁰ Grüneis, A. *et al.* Determination of two-dimensional phonon dispersion relation of graphite by Raman. *Phys. Rev. B* **65**, 155405 (2002).
- ⁵¹ Saito, R., *et al.* Probing Phonon Dispersion Relations of Graphite by Double Resonance Raman Scattering. *Phys. Rev. Lett.* **88**, 027401 (2002).
- ⁵² Kohn, W. Image of the Fermi Surface in the Vibration Spectrum of a Metal. *Phys. Rev. Lett.* **2**, 393–394 (1959).
- ⁵³ Kresse, G. *et al.* *Ab initio* Force Constant Approach to Phonon Dispersion Relations of Diamond and Graphite. *Europhys. Lett.* **32**, 729 (1995)
- ⁵⁴ Pavone, P., *et al.* *Ab initio* phonon calculations in solids. *Physica B* **219–220** 439–441 (1996).
- ⁵⁵ Dubay, O. & Kresse, G. Accurate density functional calculations for the phonon dispersion relations of graphite layer and carbon nanotubes. *Phys. Rev. B* **67**, 035401 (2003).
- ⁵⁶ Piscanec, S., Lazzeri, M., Robertson, J., Ferrari, A. C. & Mauri, F. Optical phonons in carbon nanotubes: Kohn anomalies, Peierls distortions, and dynamic effects. *Phys. Rev. B* **75**, 035427 (2007).
- ⁵⁷ Maultzsch, J., Reich, S., Thomsen, C., Requardt, H. & Ordejón, P. Phonon Dispersion in Graphite. *Phys. Rev. Lett.* **92**, 075501 (2004).
- ⁵⁸ Grüneis, A. *et al.* Phonon surface mapping of graphite: Disentangling quasi-degenerate phonon dispersions. *Phys. Rev. B* **80**, 085423 (2009).
- ⁵⁹ Pisana, S. *et al.* Breakdown of the adiabatic Born-Oppenheimer approximation in graphene. *Nature Mat.* **6**, 198–201 (2007).
- ⁶⁰ Basko, D. M. & Aleiner, I. L. Interplay of Coulomb and electron-phonon interactions in graphene. *Phys. Rev. B* **77**, 041409(R) (2008).
- ⁶¹ Maultzsch, J., Reich, S. & Thomsen, C. Double-resonant Raman scattering in graphite: Interference effects, selection rules, and phonon dispersion. *Phys. Rev. B* **70**, 155403 (2004).
- ⁶² Tan, P. H., Deng, Y. M. & Zhao, Q. Temperature-dependent Raman spectra and anomalous Raman phenomenon of highly oriented pyrolytic graphite. *Phys. Rev. B* **58**, 5435–5439 (1998).
- ⁶³ Tan, P. H. *et al.* Probing the phonon dispersions of graphite from the double-resonance process of Stokes and anti-Stokes Raman scatterings in multiwalled carbon nanotubes. *Phys. Rev. B* **66**, 245410 (2002).
- ⁶⁴ Tan, P. H., Hu, C. Y., Dong, J., Shen, W. C. & Zhang, B. F. Polarization properties, high-order Raman spectra, and frequency asymmetry between Stokes and anti-Stokes scattering of Raman modes in a graphite whisker. *Phys. Rev. B* **64**, 214301 (2001).
- ⁶⁵ Kawashima, Y. & Katagiri, G. Fundamentals, overtones, and combinations in the Raman spectrum of graphite. *Phys. Rev. B* **52**, 10053 (1995).
- ⁶⁶ Shimada, T. *et al.* Origin of the 2450 cm⁻¹ Raman bands in HOPG, single-wall and double-wall carbon nanotubes. *Carbon* **43**, 1049 (2005)
- ⁶⁷ Mafra, D. L. *et al.* Determination of LA and TO phonon dispersion relations of graphene near the Dirac point by double resonance Raman scattering. *Phys. Rev. B* **76**, 233407 (2007).
- ⁶⁸ Ferone, R., Wallbank, J. R., Zölyomi, V., McCann, E. & Fal'ko, V. I. Manifestation of LO-LA phonons in Raman scattering in graphene. *Solid State Comm.* **151**, 1071–1074 (2011).
- ⁶⁹ Venezuela, P., Lazzeri, M., and Mauri, F. Theory of double-resonant Raman spectra in graphene: intensity and line shape of defect-induced and two-phonon bands. *Phys. Rev. B* **84**, 035433 (2011).
- ⁷⁰ May, P., *et al.* Signature of the two-dimensional phonon dispersion in graphene probed by double-resonant Raman scattering. *Phys. Rev. B* **87**, 075402 (2013)
- ⁷¹ Wang, F. *et al.* Multiphonon Raman Scattering from Individual Single-Walled Carbon Nanotubes. *Phys. Rev. Lett.* **98**, 047402 (2007).
- ⁷² Reich, S., Thomsen, C. Raman spectroscopy of graphite. *Philos. Trans. R. Soc., A* **362**, 2271–2288 (2004).
- ⁷³ Basko, D. M. Calculation of the Raman *G* peak intensity in monolayer graphene: role of Ward identities. *New J. Phys.* **11**, 095011 (2009).
- ⁷⁴ Basko, D. M. Theory of resonant multiphonon Raman scattering in graphene. *Phys. Rev. B* **78**, 125418 (2008).
- ⁷⁵ Basko, D. M. Erratum: Theory of resonant multiphonon Raman scattering in graphene [Phys. Rev. B **78**, 125418 (2008)]. *Phys. Rev. B* **79**, 129902 (2008).
- ⁷⁶ Popov, V. N. & Lambin, Ph. Theoretical polarization dependence of the two-phonon double-resonant Raman spectra of graphene. *Eur. Phys. J. B* **85**, 418 (2012).
- ⁷⁷ Yoon, D. *et al.* Strong Polarization Dependence of Double-Resonant Raman Intensities in Graphene. *Nano Letters* **8**, 4270–4274 (2008).
- ⁷⁸ Song, J. C. W., Tielrooij, K. J., Koppens, F. H. L. & Levitov, L. S. Photo-excited Carrier Dynamics and Impact Excitation Cascade in Graphene. *arXiv:1209.4346*.
- ⁷⁹ Das, A. *et al.* Monitoring dopants by Raman scattering in an electrochemically top-gated graphene transistor. *Nature Nano.* **3**, 210 (2008).
- ⁸⁰ Das, A. *et al.* Phonon renormalisation in doped bilayer graphene. *Phys. Rev. B*, **79**, 155417 (2009).
- ⁸¹ Golub, L. E., Tarasenko, S. A., Entin, M. V. & Magarill, L. I. Valley separation in graphene by polarized light. *Phys. Rev. B* **84**, 195408 (2011).
- ⁸² Basko, D. M. Effect of anisotropic band curvature on carrier multiplication in graphene, *arXiv:1302.5891* (2013).
- ⁸³ Ando, T. Anomaly of Optical Phonon in Monolayer Graphene. *J. Phys. Soc. Jpn.* **75**, 124701 (2006).
- ⁸⁴ Lazzeri, M & Mauri, F. Nonadiabatic Kohn Anomaly in a Doped Graphene Monolayer. *Phys. Rev. Lett.* **97**, 266407 (2006).
- ⁸⁵ Ando, T. Magnetic Oscillation of Optical Phonon in Graphene. *J. Phys. Soc. Jpn.* **76**, 024712 (2007).
- ⁸⁶ Goerbig, M. O. *et al.* Filling-Factor-Dependent Magnetophonon Resonance in Graphene. *Phys. Rev. Lett.* **99**, 087402 (2007).

- ⁸⁷ Yan, J. *et al.* Electric Field Effect Tuning of Electron-Phonon Coupling in Graphene. *Phys. Rev. Lett.* **98**, 166802 (2007).
- ⁸⁸ Yan, J. *et al.* Observation of Anomalous Phonon Softening in Bilayer Graphene. *Phys. Rev. Lett.* **101**, 136804 (2008).
- ⁸⁹ Casiraghi, C. *et al.* Raman fingerprint of charged impurities in graphene. *Appl. Phys. Lett.* **91**, 233108 (2007).
- ⁹⁰ Kalbac, M. *et al.* The Influence of Strong Electron and Hole Doping on the Raman Intensity of Chemical Vapor-Deposition Graphene. *ACS Nano* **10** 6055-6063 (2010).
- ⁹¹ Chen, C.F. *et al.* Controlling inelastic light scattering quantum pathways in graphene. *Nature* **471**, 617-620 (2011)
- ⁹² Zhao, W. J., Tan, P. H., Liu, J. & Ferrari, A. C. Intercalation of Few-Layer Graphite Flakes with FeCl₃: Raman Determination of Fermi Level, Layer by Layer Decoupling, and Stability. *J. Am. Chem. Soc.* **133**, 5941 (2011).
- ⁹³ Sasaki, K. I., Kato, K., Tokura, Y., Suzuki, S., & Sogawa, T. Decay and Frequency Shift of Inter and Intravalley Phonons in Graphene - Dirac Cone Migration. *Phys. Rev. B* **86**, 201403(R) (2012)
- ⁹⁴ Faugeras, C. *et al.* Effect of a magnetic field on the two-phonon Raman scattering in graphene. *Phys. Rev. B* **81**, 155436 (2010).
- ⁹⁵ Faugeras, C. *et al.* Tuning the Electron-Phonon Coupling in Multilayer Graphene with Magnetic Fields. *Phys. Rev. Lett.* **103**, 186803 (2009).
- ⁹⁶ Yan J. *et al.* Observation of magneto-phonon resonance of Dirac fermions in graphite. *Phys. Rev. Lett.* **105**, 227401 (2010).
- ⁹⁷ Ando, T. Anomaly of Optical Phonons in Bilayer Graphene. *J. Phys. Soc. Japan.* **76**, 104711 (2007).
- ⁹⁸ Faugeras, C., *et al.* Probing the band structure of quadrilayer graphene with magneto-phonon resonance, *New. J. Phys.* **14** 095007 (2012).
- ⁹⁹ Kim, Y. *et al.* Filling-Factor-Dependent Magnetophonon Resonance with Circularly Polarized Phonons in Graphene Revealed by High-Field Magneto-Raman Spectroscopy. *arXiv:1211.4311* (2012).
- ¹⁰⁰ Wallace, P. R. The Band Theory of Graphite. *Phys. Rev.* **71**, 622 (1948).
- ¹⁰¹ Mucha-Kruczyński, M., Kashuba, O., and Fal'ko, V. I. Spectral features due to inter-Landau-level transitions in the Raman spectrum of bilayer graphene. *Phys. Rev. B* **82**, 045405 (2010).
- ¹⁰² Kossacki, P. *et al.* Electronic excitations and electron-phonon coupling in bulk graphite through Raman scattering in high magnetic fields. *Phys. Rev. B*, **84**, 235138, (2011)
- ¹⁰³ G. Grimvall, *Thermophysical Properties of Materials*, Holland, (1986)
- ¹⁰⁴ Mohiuddin, T. M. G. *et al.* Uniaxial Strain in Graphene by Raman Spectroscopy: G Peak Splitting, Gruneisen Parameters, and Sample Orientation. *Phys. Rev. B* **79**, 205433 (2009).
- ¹⁰⁵ Huang, M. *et al.* Phonon softening and crystallographic orientation of strained graphene studied by Raman spectroscopy. *Proc. Natl. Acad. Sci. USA* **106**, 7304-7308 (2009).
- ¹⁰⁶ Thomsen C. *et al.* Ab initio determination of the phonon deformation potentials of graphene. *Phys. Rev. B.* **65**, 073403 (2002).
- ¹⁰⁷ Sakata H. *et al.* Effect of uniaxial stress on the Raman spectra of graphite fibers. *J. Appl. Phys.* **63**, 2769 (1988).
- ¹⁰⁸ Pereira V. M, Castro Neto A. H. & Peres. N. M. R., A tight-binding approach to uniaxial strain in graphene, *Phys. Rev. B* **80**, 045401 (2009).
- ¹⁰⁹ Huang M., Hugen Y., Heinz T. F. & Hone J. Probing Strain Induced Electronic Structure Change in Graphene by Raman Spectroscopy. *Nano Lett.*, **10**, 4074-4079 (2010).
- ¹¹⁰ D. Yoon, Y. W. Son & H. Cheong. Strain-dependent Splitting of Double Resonance Raman Scattering Band in Graphene. *Phys. Rev. Lett.* **106**, 155502 (2011).
- ¹¹¹ Proctor J. E. *et al.* Graphene under hydrostatic pressure. *Phys. Rev. B* **80**, 073408 (2009)
- ¹¹² Cowley R. A., Anarmonic Crystals. *Rep. Prog. Phys.* **31**, 123 (1968).
- ¹¹³ Balkanski, M., Wallis, R. F. & Haro, E. *Phys. Rev. B* **28**, 1928 (1983).
- ¹¹⁴ Cai, W. W., *et al.* Synthesis and solid-state nmr structural characterization of C¹³ labeled graphite oxide. *Science* **321** 1815, (2008)
- ¹¹⁵ Chen, J. H., Cullen, W. G., Jang, C., Fuhrer, M. S. & Williams E. D. Defect scattering in graphene. *Phys. Rev. Lett.* **102**, 236805 (2009)
- ¹¹⁶ Ni, Z., Ponomarenko, L., Nair, R., Yang, R., Anissimova, S., Grigorieva, I., Schedin, F., Blake, P., Shen, Z., Hill, E., Novoselov, K. S. & Geim, A. K. On resonant scatterers as a factor limiting carrier mobility in graphene. *Nano Lett.* **10**, 3868-3872 (2010).
- ¹¹⁷ Freitag M. *et al.*, Energy dissipation in graphene field-effect transistors. *Nano Lett.* **9**, 1883 (2009)
- ¹¹⁸ Balandin, A. A. *et al.* Superior Thermal Conductivity of Single-Layer Graphene. *Nano Lett.* **8**, 902 (2008)
- ¹¹⁹ Balandin, A. A. Thermal properties of graphene and nanostructured carbon materials. *Nature Materials* **10**, 569 (2011)
- ¹²⁰ Elias, D. C. *et al.* Control of Graphene's Properties by Reversible Hydrogenation: Evidence for Graphane. *Science*, **323**, 610-613 (2009).
- ¹²¹ Gokus, T. *et al.* Making Graphene Luminescent by Oxygen Plasma Treatment. *ACS Nano* **3**, 3963-3968 (2009).
- ¹²² Ferrari, A. C. *et al.* Interpretation of infrared and Raman spectra of amorphous carbon nitrides. *Phys. Rev. B* **67**, 155306 (2003).